CLUSTALW (ref. 21); the resulting alignments were manually inspected using the ED program from the MUST package[22]. Only unambiguously aligned positions were used in phylogenetic analyses. A fusion F1 was built for 12 operational taxonomic units (OTUs) (Fig. 2) by concatenation of the 13 proteins (5,171 sites: 1,597 constant, 3,574 polymorphic). A fusion F2 (1,938 sites: 672 constant, 1,266 polymorphic) was constructed to include the glaucophyte *C. paradoxa*. It contained data from 6 proteins (actin, α-tubulin, β-tubulin, EF-1α, Hsp70 and ATPase vatB) and 13 OTUs (Fig. 2b). Fusion alignments and accession numbers for all sequences used are given in Supplementary Information.

Distance, MP and ML analyses were carried out with all individual and concatenated data sets using MUST (ref. 22), PAUP 3.1 (ref. 23), and PROTML 2.3 (ref. 24), respectively. To carry out exhaustive ML analyses of all possible tree topologies, several constraints were imposed to reduce the number of possible trees (see Figs 1 and 2). Calculation of α-parameter values and other ML analyses taking into account ASRV were conducted using the program PUZZLE (ref. 25). Maximum-likelihood bootstrap proportions were computed using the RELL method[26] upon the 5,000 top-ranking trees. For distance and parsimony analyses, 1,000 bootstrap replicates were computed. Kishino–Hasegawa tests[14] were carried out comparing ln*L* of the best 50 trees containing monophyletic GR with ln*L* of the best 50 trees without monophyletic GR, using PROTML 2.3 (ref. 24) (without considering ASRV) and PUZZLE[25] (with a Γ-law to correct for ASRV). In the case of fusion F2, we used Kishino–Hasegawa tests to estimate the Δ ln*L* between the best 50 trees containing monophyletic GR + Glaucophyta and the best 50 trees without this monophyletic group.

Received 22 December 1999; accepted 29 February 2000.

1. Douglas, S. E. Plastid evolution: origins, diversity, trends. *Curr. Opin. Genet. Dev.* **8,** 655–661 (1998).
2. Burger, G., Saint-Louis, D., Gray, M. W. & Lang, B. F. Complete sequence of the mitochondrial DNA of the red alga *Porphyra purpurea*. Cyanobacterial introns and shared ancestry of red and green algae. *Plant Cell* **11,** 1675–1694 (1999).
3. Ragan, M. & Gutell, R. Are red algae plants? *Bot. J. Linn. Soc.* **118,** 81–105 (1995).
4. Stiller, J. W. & Hall, B. D. The origin of red algae: implications for plastid evolution. *Proc. Natl Acad. Sci. USA* **94,** 4520–4525 (1997).
5. Cavalier-Smith, T. Eukaryote kingdoms: seven or nine? *Biosystems* **14,** 461–481 (1981).
6. Martin, W. *et al.* Gene transfer to the nucleus and the evolution of chloroplasts. *Nature* **393,** 162–165 (1998).
7. Kumar, S. & Rzhetsky, A. Evolutionary relationships of eukaryotic kingdoms. *J. Mol. Evol.* **42,** 183–193 (1996).
8. Bhattacharya, D. & Weber, K. The actin gene of the glaucocystophyte *Cyanophora paradoxa*: analysis of the coding region and introns, and an actin phylogeny of eukaryotes. *Curr. Genet.* **31,** 439–446 (1997).
9. Philippe, H. & Laurent, J. How good are deep phylogenetic trees? *Curr. Opin. Genet. Dev.* **8,** 616–623 (1998).
10. Swofford, D. L., Olsen, G. J., Waddell, P. J. & Hillis, D. M. in *Molecular Systematics* (eds Hillis, D. M., Moritz, C. & Mable, B. K.) 407–514 (Sinauer Associates, Sunderland, Massachusetts, 1996).
11. Hirt, R. P. *et al.* Microsporidia are related to fungi: evidence from the largest subunit of RNA polymerase II and other proteins. *Proc. Natl Acad. Sci. USA* **96,** 580–585 (1999).
12. Fabrizio, P., Laggerbauer, B., Lauber, J., Lane, W. S. & Luhrmann, R. An evolutionarily conserved U5 snRNP-specific protein is a GTP-binding factor closely related to the ribosomal translocase EF-2. *EMBO J.* **16,** 4092–4106 (1997).
13. Embley, T. M. & Hirt, R. P. Early branching eukaryotes? *Curr. Opin. Genet. Dev.* **8,** 624–629 (1998).
14. Kishino, H. & Hasegawa, M. Evaluation of the maximum likelihood estimate of the evolutionary tree topologies from DNA sequence data, and the branching order in hominoidea. *J. Mol. Evol.* **29,** 170–179 (1989).
15. Graybeal, A. Is it better to add taxa or characters to a difficult phylogenetic problem? *Syst. Biol.* **47,** 9–17 (1998).
16. Hillis, D. M. Inferring complex phylogenies. *Nature* **383,** 130–131 (1996).
17. Bhattacharya, D. & Schmidt, H. A. in *Origins of Algae and Their Plastids* (ed. Bhattacharya, D.) 139–148 (Springer, Vienna, New York, 1997).
18. Moreira, D. Efficient removal of PCR inhibitors using agarose-embedded DNA preparations. *Nucleic Acids Res.* **26,** 3309–3310 (1998).
19. Yamamoto, A., Hashimoto, T., Asaga, E., Hasegawa, M. & Goto, N. Phylogenetic position of the mitochondrion-lacking protozoan *Trichomonas tenax*, based on amino acid sequences of elongation factors 1alpha and 2. *J. Mol. Evol.* **44,** 98–105 (1997).
20. Altschul, S. F., Gish, W., Miller, W., Myers, E. W. & Lipman, D. J. Basic local alignment search tool. *J. Mol. Biol.* **215,** 403–410 (1990).
21. Thompson, J. D., Higgins, D. G. & Gibson, T. J. CLUSTAL W: improving the sensitivity of progressive multiple sequence alignment through sequence weighting, position-specific gap penalties and weight matrix choice. *Nucleic Acids Res.* **22,** 4673–4680 (1994).
22. Philippe, H. MUST, a computer package of management utilities for sequences and trees. *Nucleic Acids Res.* **21,** 5264–5272 (1993).
23. Swofford, D. L. PAUP: phylogenetic analysis using parsimony. Version 3.1.1. (Illinois Natural History Survey, Champaign, 1993).
24. Adachi, J. & Hasegawa, M. MOLPHY version 2. 3: programs for molecular phylogenetics based on maximum likelihood. *Comput. Sci. Monogr.* **28,** 1–150 (1996).
25. Strimmer, K. & von Haeseler, A. Quartet puzzling: a quartet maximum likelihood method for reconstructing tree topologies. *Mol. Biol. Evol.* **13,** 964–969 (1996).
26. Kishino, H., Miyata, T. & Hasegawa, M. Maximum likelihood inference of protein phylogeny, and the origin of chloroplasts. *J. Mol. Evol.* **31,** 151–160 (1990).

Supplementary information is available on *Nature*'s World-Wide Web site (http://www.nature.com) or as paper copy from the London editorial office of *Nature*.

Acknowledgements

We thank P. Lopez, P. López-García and M. Müller for critical reading of the manuscript; C. R. Engel for DNA samples; G. Fryd for cultures; N. Narradon for technical help; and the Kazusa Institute, Marine Biological Laboratory, Sanger Centre, Stanford Centre, the Institute of Genomic Research and Tsukuba Laboratory for access to sequence data. D. M. is the recipient of a stipend from the Fondation des Treilles.

Correspondence and request for materials should be addressed to D. M. (e-mail: david.moreira@bc4.u-psud.fr). EF-2 sequences have been deposited in GenBank under accession numbers AF213661, AF213662 AF213663, AF213664 and AF213665.

Encoding of movement time by populations of cerebellar Purkinje cells

Peter Thier*, Peter W. Dicke*, Roman Haas* & Shabtai Barash†

* *Department of Cognitive Neurology, University of Tübingen, Hoppe-Seyler-Straße 3, 72076 Tübingen, Germany*
† *Department of Neurobiology, The Weizmann Institute, 76100 Rehovot, Israel*

One of the earliest computational principles attributed to the cerebellum was the measurement of time[1]. This idea was originally suggested on anatomical grounds, and was taken up again to explain some of the deficits in cerebellar patients[2,3]. The contribution of the cerebellum to eye movements, in contrast, has traditionally been discussed in the context of motor learning[4–7]. This view has received support from the loss of saccade adaptation, one of the key examples of motor learning, following lesions of the posterior cerebellar vermis[8–11]. However, the relationship between the properties of saccade-related vermal Purkinje cells and the behavioural deficits that follow lesions is unclear. Here we report results from single-unit recording experiments on monkeys that reconcile the seemingly unrelated concepts of timing and motor learning. We report that, unlike individual Purkinje cells, the population response of larger groups of Purkinje cells gives a precise temporal signature of saccade onset and offset. Thus a vermal population response may help to determine saccade duration. Modifying the time course of the population response by changing the weights of the contributing individual Purkinje cells, discharging at different times relative to the saccade, would directly translate into changes in saccade amplitude.

We recorded extracellularly from 131 saccade-related Purkinje cells (PCs) in vermal lobuli VI and VIIA of two rhesus monkeys, while the animals performed visually guided saccades. The preferred direction was determined by asking the monkeys to make 15° centre-out saccades in eight directions. As in previous work on saccade-related responses in the oculomotor vermis[12–15], these saccade-related responses were characterized by bursts of activity in tight temporal relationship with the execution of a saccade in particular preferred directions (Fig. 1). Only a few PCs (5/131) with saccade-related bursts lacked this directional preference. To ensure that the saccade-related bursts did not reflect a visual response evoked by the peripheral target, we tested 98 of the PCs considered on a 'memory saccade' task, separating the presentation of the peripheral target and the saccade in time. The monkeys were asked to saccade to a remembered location in the frontoparallel plane, cued by the brief presentation of a peripheral target. Of the 98 PCs tested, 71 lacked a significant visual response to the presentation of the peripheral cue in this memory saccade task and only five showed a visual response reaching 50% or more of the later saccade-related burst.

The tight alignment of saccade-related bursts exhibited by many of the PCs with the saccades indicated that vermal PCs might help to

determine the timing of saccades. We therefore investigated whether single PC bursts predict saccade duration. To obtain saccades with sufficiently variable durations for each neuron, we exploited the fact that saccade duration increases monotonically with saccade amplitude[16] (Fig. 2a). We collected responses to saccades of different amplitudes, from 5° to 40°, all in a PC's best direction (or alternatively a fixed direction for non-directional cells). Figure 1 shows the responses of four different PCs, exemplifying the different dependencies of responses on saccade amplitude exhibited by vermal PCs. Some vermal PCs (Fig. 1a) showed clear preferences for specific saccade amplitudes (about 20° in this example) with increasingly weaker responses for amplitudes deviating increasingly from the optimum. Other PCs (Fig. 1b, c) displayed no or little influence of saccade amplitude. Still others (Fig. 1d) showed a monotonic dependence of response on saccade amplitude. To characterize the dependence of saccade-related bursts of vermal PCs on saccade amplitude or duration, we computed several parameters characterizing the saccade-related bursts of each cell.

Figure 2 shows the means and standard errors of the parameters considered for the 94 PCs for which amplitude-tuning data was available. The mean burst onset latency, relative to saccade onset, did not depend on saccade duration (Fig. 2b). The burst offset latency increased with saccade duration (Fig. 2c). Consequently, the mean burst duration increased with saccade duration (Fig. 2d). As the mean discharge rate in the burst did not depend significantly on saccade duration (Fig. 2e), the increase in burst duration with saccade duration must fully account for the modest increase in the mean number of spikes (Fig. 2f). These results may indicate that the timing of the PC bursts reflects the timing of the saccade: certainly, the mean firing rate, computed over the whole burst, carries no information (Fig. 2e). However, the variability of the data, conveyed by the very large errors of the means, confounds the interpretation of Fig. 2. This variability is likely to be caused, in part, by the procedure of first deriving parameters for each PC and then analysing these parameters rather than deriving parameters from the whole sample of responses in one step.

Any biologically plausible mechanism involved in extracting information from a larger group of PCs is likely to be sensitive to the timing of individual bursts and even the timing of individual spikes. We therefore investigated whether the collective instantaneous discharge rate of all PCs in the sample might reflect more faithfully saccade duration or other aspects of saccade timing. Figure 3a shows the collective saccade-related instantaneous discharge rate, henceforth referred to as the population burst, as a function of saccade duration. It was computed by sorting the saccade-related responses of the cells whose responses were

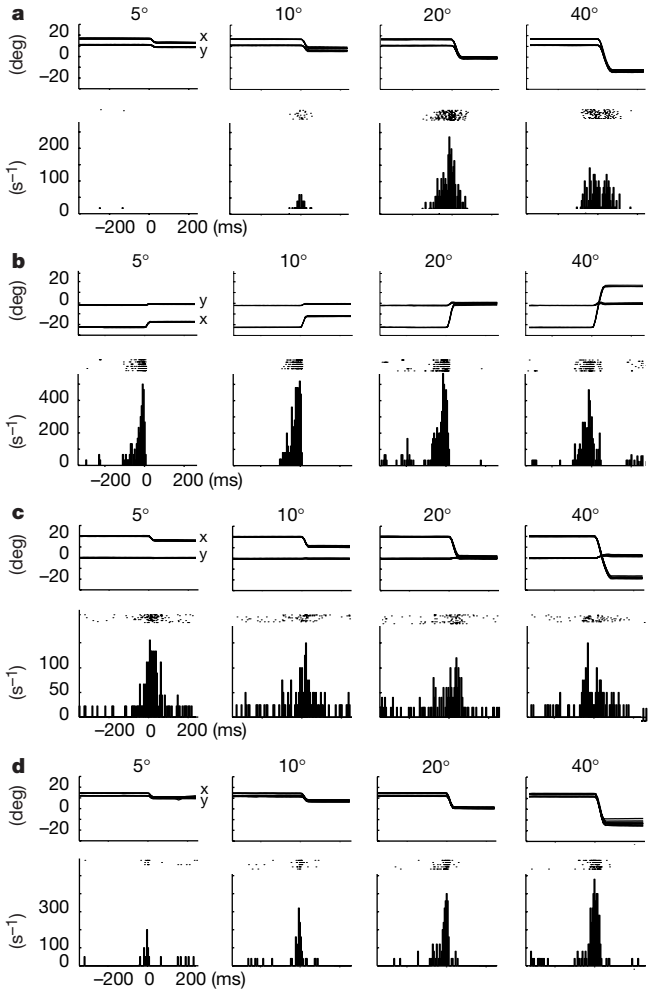

Figure 1 Perisaccadic time histograms and raster plots obtained from vermal PCs, reflecting the highly variable dependence of saccade-related bursts on saccade amplitude. **a–d**, Four individual PCs. *x*, *y*: horizontal and vertical components of eye position. Width of time bins, 5 ms.

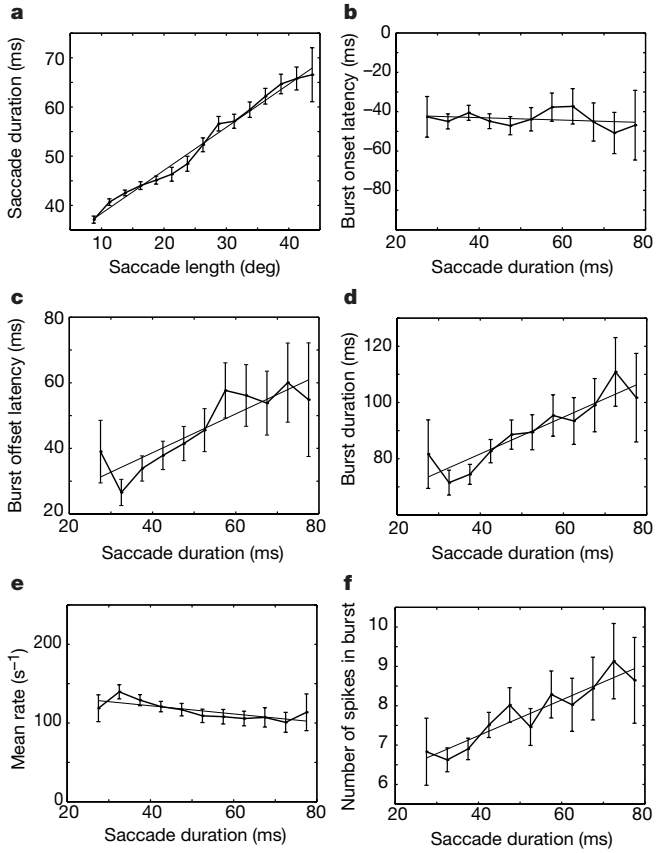

Figure 2 Dependence of saccade duration on saccade length (**a**) and burst parameters on saccade durations (**b–f**). **a**, Mean saccade duration as a function of saccade length, based on eye movement records collected with the 94 single units whose amplitude tuning was studied. Vertical bars, s.e. Saccade duration increases linearly with saccade amplitude (thin line; slope $m = 0.875$; $P < 10^{-12}$). **b–f**, Dependence of various features of saccade-related bursts of vermal PCs on saccade duration. The plots show mean ± s.e. The three variables that showed a significant (linear regression (thin lines), $P < 0.05$) but modest dependence on saccade duration were burst offset latency (**c**, $P < 0.00031$), burst duration (**d**, $P < 0.0077$) and the overall number of spikes in the burst (**f**, $P < 0.0031$).

characterized in Fig. 2, according to saccade duration (bin width 2.5 ms). Next, for each saccade duration, we computed compound perisaccadic histograms with a bin-width of 1 ms, smoothed by a gaussian filter with a standard deviation of 10 ms. These compound perisaccadic histograms were then plotted as function of saccade duration, aligned relative to saccade onset for each of the eight directions tested, and the mean of the plots for the individual directions was taken as the estimate of the population burst.

The population burst is shown in Fig. 3a as it develops over time (x-axis) for saccades of duration 30–65 ms (y-axis). The upper part of Fig. 3b displays three individual sections through the colour-coded plot shown in Fig. 3a, illustrating population bursts for saccades of 30, 49 and 65 ms, respectively. The population response, independent of saccade duration, starts to rise above the baseline level before saccade onset, peaks at saccade onset, and then declines again and reaches the baseline level when the saccade ends (Fig. 3a, b).

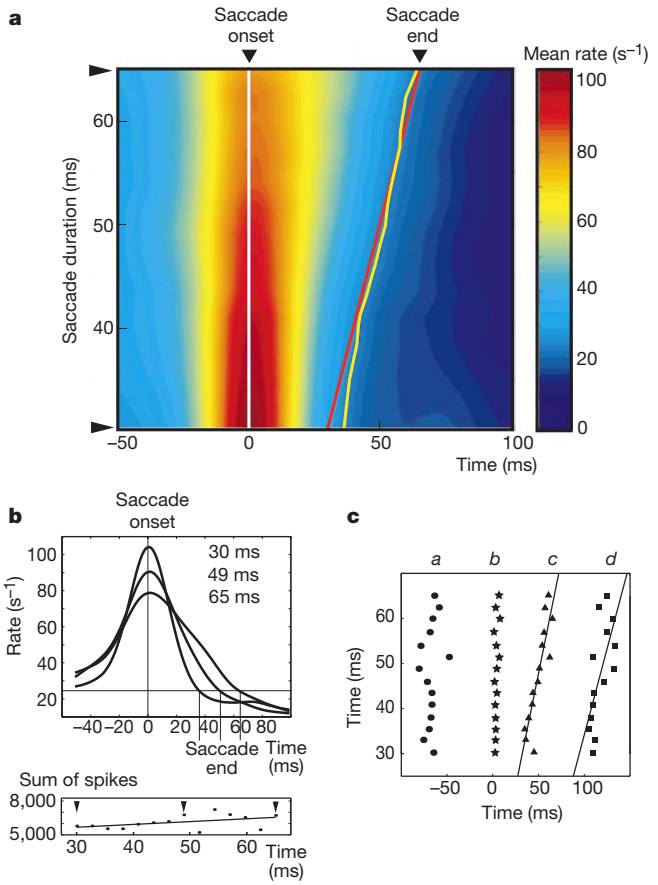

Figure 3 Dependence of the population burst on saccade duration. **a**, Population burst (94 vermal saccade-related PCs) plotted as a function of saccade time (x-axis; 0, saccade onset) and duration (y-axis), measured in discrete time steps (x-axis: 1 ms, y-axis: 2.5 ms). We used a gaussian filter (s.d. 10 ms) to smooth the plot along the x-axis and a Savitzky–Golay filter[29] (*window* = 3; deg = 1) along the y-axis. Yellow line, population activity four times the mean baseline activity (6 spikes s^{-1}; see Methods). **b**, Top, population burst profiles represent sections through the three-dimensional plot shown in **a** at individual saccade durations of 30, 49 and 65 ms. Bottom, linear regression on the overall number of spikes in the population burst, as a function of saccade duration, revealed no significant dependence ($P > 0.05$). **c**, Plots of time t as a function of: a, population burst onset latency; b, time to peak; c, time at end; and d, population burst duration (c-a). Burst onset and burst end are defined by a 4 × baseline criterion (see text). In the case of a, b and d, t is saccade duration; in the case of c, t is the time of saccade termination. Both c and d increase significantly with t ($t = 1.0138c - 3.9389$, $P < 0.0028$; $t = 0.7636d - 42.333$, $P < 0.01$; the slopes for c and d are significantly different, $P < 0.031$), whereas neither a nor b depends on saccade duration ($P > 0.05$).

To relate the time course of the population burst more precisely to the time course of the saccade, we determined the times of onset (a), peak (b) and offset (c) of the population burst relative to saccade onset for each saccade duration as well as the population burst duration (d), defined as c-a. We defined population burst onset and offset times as the times when the population burst reached four times the baseline firing rate when building up and when declining. Figure 3c plots time t as function of a, b, c and d, respectively. In the case of a, b and d, t corresponds to saccade duration, in the case of c to the time of saccade termination. The plots were fitted by linear regressions. Both c and d increased linearly (c: $P < 0.00003$, d: $P < 0.01$) with the time of saccade termination and saccade duration, respectively, whereas neither a nor b depended significantly ($P > 0.05$) on saccade duration. The population burst onset leads the saccade onset by 67.9 ± 8.25 ms, whereas the population burst peak appears roughly at the time of saccade onset (2.78 ± 1.97 ms), both independent of saccade duration. The end of the population burst (c), as predicted by the regression, corresponds very closely to the end of the saccade, whereas the population burst duration (d) underestimates saccade duration by 24% (Fig. 3c). This and the significantly higher coefficient of correlation ($P < 0.004$) for c compared with d indicate that the population burst reflects the time of saccade termination rather than saccade duration.

Although the peak of the population burst would be too late to be causally related to saccade onset, its precise alignment with saccade onset might be understood as reflecting the zeroing of the 'stop-watch', determining the termination of the saccade. In accordance with this model, the interval $e = c$-b between the population burst peak b and the population burst offset c gives a fairly accurate account of saccade duration t (linear regression: $t = 1.121e$-5.126; $P < 0.0046$). The population burst peak is characterized by a second conspicuous feature, a decrease in its peak amplitude pa with saccade duration t (linear regression, $pa = -0.81t + 130.751$; $P < 0.0244$; Fig. 3b). This decrease accompanies an increase in the width of the population burst with increasing saccade duration. These two dependencies combine to leave the overall number of spikes in the population burst largely independent of saccade duration (Fig. 3b, lower). Thus, the decrease in peak firing rate with saccade duration might simply reflect the need to redistribute an approximately constant number of spikes over varying segments of time. Alternatively,

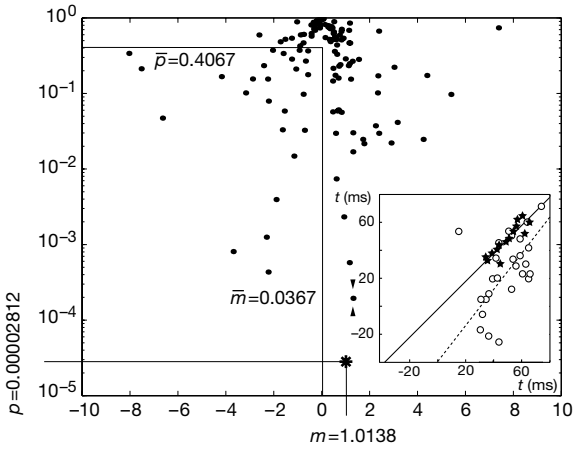

Figure 4 Scatter-plot of p, the probability of the linear regression, fitting plots of saccade end as function of burst end, as a function of its slope m. The dots give the p, m coordinates of individual PCs and the asterisk indicates the p, m coordinate of the population response. The inset compares the regression analyses for the population burst and the 'best' PC (marked by two arrowheads), singled out by the smallest p and an m close to the ideal of 1. The x-axis plots time with $t = 0$ corresponding to saccade onset. The y-axis plots the time of the burst end relative to saccade onset.

the peak firing rate might encode dynamic saccade parameters, which, like saccade velocity, depend on saccade duration[16]. Such a putative dependence between peak firing rate and saccade velocity would be specific to the population burst, not shared by individual cells. Both the peak discharge rates and the mean discharge rates in the saccade-related bursts are on average independent of saccade velocity (linear regression analysis, $P > 0.05$). Notwithstanding the question of whether the amplitude of the peak population burst has a function, the timing of the burst is independent of and cannot be explained by the amplitude of the peak population burst.

The faithful description of saccade timing provided by the population burst could reflect the contribution of a subgroup of 'best' PCs or, alternatively, emerge as a true *de novo* feature of the population response. To distinguish between these possibilities, we compared the linear regression for the plot of burst end (c) based on the population burst as shown in Fig. 3c with the corresponding linear regressions for individual PCs. Figure 4 shows the significance level p of the linear regressions as a function of their slopes m. An m of 1 would reflect a faithful representation of saccade end. The slope of the regression plotting saccade end as a function of the population burst end comes very close to this ideal ($m = 1.0138$). On the other hand, the m for the individual PCs is on average close to zero and varies widely ($m_{\text{mean}} = 0.0367 \pm 2.0054$). Moreover, even the best of the individual regressions is not nearly as good, as measured by their m and p coordinates, as the one for the population burst. This is shown in the inset, which compares the regression for the population burst with the regression for the 'best' cell (singled out by arrows in the $p(m)$ plot). In summary, this analysis indicates that the population burst reflects the timing of saccade termination and that this precise reflection is a *de novo* property of the population response, rather than a reflection of the properties of the 'best' PCs.

Does cerebellar population encoding for saccades do more than alleviate the insufficiencies of individual cells? We propose that it could make an important contribution to saccadic plasticity. If we assume that the end of the population burst determines the end of the saccade, a simple way to make a too-small saccade normometric would be to increase the duration of the population response. The necessary increase in the duration of the population response could be achieved by increasing the gain of relatively 'late' vermal PCs, based on an appropriate error signal. There are three findings that support this hypothesis. First, adaptive modification of saccades in humans leads to a selective activation of those parts of the human cerebellum that are probably homologous to the monkey oculomotor vermis[17]. Second, the capacity for rapid saccadic plasticity is irreversibly lost following lesions of the posterior vermis in monkeys[10]. And finally, some saccade-related neurons in the caudal fastigial nucleus (cFN), which are controlled by vermal PCs[18–20], show bursts that occurr later if saccades are modified so as to become larger for a given retinal vector[21]. A putative function of this type of cFN burst is the braking of ongoing saccades, and a likely mechanism underlying these bursts is release from PC inhibition, giving rise to a rebound depolarisation[22,23]. Hence, learning to make larger saccades would involve a sequence of prolonged vermal PC inhibition and a delayed fastigial rebound, ultimately translating into a delayed braking signal for saccades.

Obviously, this scheme, which tries to lead saccadic learning back to an optimization of a representation of time, is not confined to the saccadic system. Rather, it might be applicable to any motor or non-motor function that is dependent on the availability of a precise representation of time. □

Methods

We recorded extracellularly from lobuli VI and VIIA of the posterior vermis of one female and one male rhesus monkey (P and S) while they performed visually guided saccades, evoked by asking the monkeys to saccade to peripheral cues that appeared when the fixation spot disappeared. The monkeys were prepared for chronic single unit and eye position recordings, the latter based on the search coil technique, as described[24,25]. All animal procedures followed the guidelines set by the NIH and national law and were approved by the local committee supervising the handling of experimental animals. Recording site localization in lobuli VI and VIIA relied on stereotactic calculations based on postsurgical MRI scans, which showed both these brainstem structures as well as the precise location and orientation of the implanted recording chamber. A conventional reconstruction of recording sites based on post-mortem brain sections was carried out in monkey P. In perfect correspondence with the tentative localization based on MRI, recording sites were confined to lobuli VI and VIIA. Well isolated single units encountered in lobuli VI and VIIA were interpreted as reflecting PCs, without first trying to identify complex spikes. This simplified approach seemed acceptable in view of our previous experience[26]: using the same type of microelectrode, we found that the vermal single units analysed ($n = 56$) all exhibited complex spikes, identifying them as Purkinje cells.

The preferred direction of a neuron was studied by measuring responses to visually guided saccades of 15° or 20° amplitude in eight equally spaced directions (0°, 45° and so on) in the frontoparallel plane, starting from straight ahead. A response was considered to be directionally selective if the mean number of spikes in the best direction was at least twice the response in the worst direction. To reveal visual contamination of saccade-related responses, we next ran a standard centre-out memory saccade task. A location in the frontoparallel plane was cued by the presentation of a peripheral target 600–800 ms after the start of the trial, while the monkey fixated a central spot. The disappearance of the central fixation spot, 700 ms after the disappearance of the peripheral cue, served as the go signal for the saccade. Target locations of memory guided saccades corresponded to those of visually guided saccades.

The visual response to the peripheral target was estimated by calculating the mean discharge rate in a window from 670 to 800 ms. The visual response was considered to be significant if it exceeded the baseline discharge rate plus two s.d. Finally, the amplitude or duration tuning of a PC was determined by asking the monkey to make saccades of varying amplitudes from 2.5° (or 5° in some cases) to 40° in steps of 2.5–5° in the neuron's preferred direction. Amplitudes were presented randomly interleaved. As the field of view was limited to 50° × 45° by the monitor on which stimuli were presented, the starting point of saccade vectors larger than 20° had to be moved to eccentric locations, in a direction opposite to saccade directions. Starting saccades from different orbital positions was allowed, as our own work suggests that, contrary to earlier reports, the influence of the orbital starting position on saccade-related responses of posterior vermal PCs is indeed negligible[26,27]. The start and end of saccade-related PC bursts were determined in single trials by applying a Poisson spike train analysis[28] with a confidence level of usually $P < 0.05$ ($P < 0.1$ in a few cases). To exclude spurious bursts, we used the following qualifications: burst onset had to follow the extinction of the fixation point; and burst onset had to be within a period starting 150 ms before saccade onset and lasting until the end of the saccade. Additional bursts following the first one were detected in case the first burst ended before the end of the saccade. The baseline activity rate was estimated as the mean discharge rate from −400 to −100 ms (memory saccades) or −300 to −100 ms (visually guided saccades) relative to the onset of the peripheral target.

Received 7 December 1999; accepted 18 February 2000.

1. Braitenberg, V. Functional interpretation of cerebellar histology. *Nature* **190,** 539–640 (1961).
2. Ivry, R. B. & Diener, H. C. Impaired velocity perception in patients with lesions of the cerebellum. *J. Cogn. Neurosci.* **3,** 355–366 (1991).
3. Ivry, R. B. & Keele, S. W. Timing functions of the cerebellum. *J. Cogn. Neurosci.* **1,** 136–152 (1993).
4. Marr, D. A theory of cerebellar cortex. *J. Physiol.* **202,** 437–470 (1969).
5. Ito, M. Cerebellar control of the vestibulo-ocular reflex- around the flocculus hypothesis. *Annu. Rev. Neurosci.* **5,** 275–296 (1982).
6. Kawato, M. & Gomi, H. The cerebellum and VOR/OKR learning models. *Trends Neurosci.* **15,** 445–453 (1992).
7. Raymond, J. L., Lisberger, S. G. & Mauk, M. D. The cerebellum: A neuronal learning machine? *Science* **272,** 1126–1131 (1996).
8. Optican, L. M. & Robinson, D. A. Cerebellar-dependent adaptive control of primate saccadic system. *J. Neurophysiol.* **44,** 1058–1076 (1980).
9. Takagi, M., Zee, D. S. & Tamargo, R. J. Effects of lesions of the oculomotor vermis on eye movement in primate: saccades. *J. Neurophysiol.* **80,** 1911–1931 (1998).
10. Barash, S. *et al.* Saccadic dysmetria and adaptation after lesions of the cerebellar cortex. *J. Neurosci.* **19,** 10931–10939 (1999).
11. Fitzgibbon, E. J. & Goldberg, R. A. in *Adaptive Processes in Visual and Oculomotor Systems* (eds Keller, B. L. & Zee, D. S.) 329–333 (Pergamon, Oxford, 1986).
12. Llinás, R. & Wolfe, J. W. Functional linkage between the electrical activity in the vermal cerebellar cortex and saccadic eye movements. *Exp. Brain Res.* **29,** 1–14 (1977).
13. Kase, M., Miller, D. C. & Noda, H. Discharges of Purkinje cells and mossy fibers in the cerebellar vermis of the monkey during saccadic eye movements and fixation. *J. Physiol. (Lond.)* **300,** 539–555 (1980).
14. Sato, H. & Noda, H. Posterior vermal Purkinje cells in macaques responding during saccades, smooth pursuit, chair rotation and/or optokinetic stimulation. *Neurosci. Res.* **12,** 583–595 (1992).
15. Helmchen, C. & Büttner, U. Saccade-related Purkinje cell activity in the oculomotor vermis during spontaneous eye movements in light and darkness. *Exp. Brain Res.* **103,** 198–208 (1995).
16. Bahill, A. T., Clark, S. A. & Stark, R. J. The main sequence, a tool for studying human eye movements. *Math. Biosci.* **24,** 287–298 (1975).
17. Desmurget, M. *et al.* Functional anatomy of saccadic adaptation in humans. *Nature Neurosci.* **1,** 524–528 (1998).
18. Ohtsuka, K. & Noda, H. Saccadic burst neurons in the oculomotor region of the fastigial nucleus of macaque monkey. *J. Neurophysiol.* **65,** 1422–1434 (1991).
19. Fuchs, A. F., Robinson, F. R. & Straube, A. Role of caudal fastigial nucleus in saccade generation. I. Neuronal discharge patterns. *J. Neurophysiol.* **70,** 1723–1740 (1993).
20. Noda, H., Sugita, S. & Ikeda, Y. Afferent and efferent connections of the oculomotor region of the fastigial nucleus in the macaque monkey. *J. Comp. Neurol.* **302,** 330–348 (1990).
21. Scudder, C. A. Discharge of fastigial nucleus neurons is altered during adaptive modification of

saccade size. *Soc. Neurosci. Abstr.* **24,** 147 (1998).
22. Llinás, R. & Mühlethaler, M. Electrophysiology of guinea-pig cerebellar nuclear cells in the *in vitro* brain stem–cerebellar preparation. *J. Physiol. (Lond.)* **404,** 241–258 (1988).
23. Aizenmann, C. D. & Linden, D. J. Regulation of the rebound depolarization and spontaneous firing patterns of deep nuclear neurons in slices of rat cerebellum. *J. Neurophysiol.* **82,** 1697–1709 (1999).
24. Judge, S. J., Richmond, B. J. & Chu, F. C. Implantation of magnetic search coils for measurement of eye position: an improved method. *Vision Res.* **20,** 535–538 (1980).
25. Thier, P. & Erickson, R. G. Responses of visual-tracking neurons from cortical area MSTl to visual, eye and head motion. *Eur. J. Neurosci.* **4,** 539–553 (1992).
26. Thielert, C.-D. *Elektrophysiologische und Anatomische Untersuchungen zum Okulomotorischen Beitrag des Posterioren Vermis des Rhesusaffen.* Thesis, Eberhard-Karls-Universität Tübingen (1996).
27. Haas, R., Dicke, P. W. & Thier, P. Saccade-related responses of most posterior vermal Purkinje cells do not depend on the starting position of the eyes. *Soc. Neurosci. Abstr.* **25,** 1652 (1999).
28. Hanes, D. P., Thompson, K. G. & Schall, J. D. Relationship of presaccadic activity in frontal eye field and supplementary eye field to saccade initiation in macaque: Poisson spike train analysis. *Exp. Brain Res.* **103,** 85–96 (1995).
29. Press, H. W., Teukolsky, S. A., Vetterling, W. T. & Flannery, B. P. (eds) *Numerical Recipes in C*, 650–655 (Cambridge Univ. Press, Cambridge, 1992).

Acknowledgements

This work was funded by the German-Israeli-Foundation and the German Research Council (Forschergruppe 'Wahrnehmen und Agieren im Raum'). We thank M. Erb and W. Grodd for their help with the anatomic MRI scans and C. Schwarz and F. Sultan for helpful comments on an earlier version of the manuscript.

Correspondence and requests for materials should be addressed to P.T. (e-mail: thier@uni-tuebingen.de).

Silberblick/Wnt11 mediates convergent extension movements during zebrafish gastrulation

Carl-Philipp Heisenberg*†, Masazumi Tada†‡, Gerd-Jörg Rauch§, Leonor Saúde‡, Miguel L. Concha*, Robert Geisler§, Derek L. Stemple‡, James C. Smith‡ & Stephen W. Wilson*

** Department of Anatomy and Developmental Biology, University College London, Gower Street, London WC1E 6BT, UK*
‡ Division of Developmental Biology, National Institute for Medical Research, The Ridgeway, Mill Hill, London NW7 1AA, UK
§ Abteilung Genetik, Max-Planck-Institut für Entwicklungsbiologie, Spemannstrasse 35, D-72076 Tübingen, Germany
† These authors contributed equally to this work

Vertebrate gastrulation involves the specification and coordinated movement of large populations of cells that give rise to the ectodermal, mesodermal and endodermal germ layers. Although many of the genes involved in the specification of cell identity during this process have been identified, little is known of the genes that coordinate cell movement. Here we show that the zebrafish *silberblick* (*slb*) locus[1] encodes Wnt11 and that Slb/Wnt11 activity is required for cells to undergo correct convergent extension movements during gastrulation. In the absence of Slb/Wnt11 function, abnormal extension of axial tissue results in cyclopia and other midline defects in the head[2]. The requirement for Slb/Wnt11 is cell non-autonomous, and our results indicate that the correct extension of axial tissue is at least partly dependent on medio-lateral cell intercalation in paraxial tissue. We also show that the *slb* phenotype is rescued by a truncated form of Dishevelled that does not signal through the canonical Wnt pathway[3], suggesting that, as in flies[4], Wnt signalling might mediate morphogenetic events through a divergent signal transduction cascade. Our results provide genetic and experimental evidence that Wnt activity in lateral tissues has a crucial role in driving the convergent extension movements underlying vertebrate gastrulation.

Vertebrate gastrulation is driven by coordinated morphogenetic movements of the three germ layers: ectoderm, mesoderm and endoderm. During this process, convergent extension movements within the mesoderm are generated by polarization of mesodermal cells followed by medio-lateral cell intercalation, which causes cells to become distributed along the antero-posterior axis[5,6]. Several mutants exhibiting defective gastrulation movements have been identified in zebrafish[7,8]. In *slb* mutants, extension of the axial mesendoderm and overlying ventral central nervous system is disturbed, resulting in fusion of the eyes later in development[2]. As previous results have suggested that Wnt activity and especially Wnt11 might affect the movement of cells during gastrulation[3,9–11], it seemed possible that mutations in Wnt11 might underlie the *slb* phenotype. Mapping of *slb* and *wnt11* showed both to be located at a similar position on linkage group 5 (Fig. 1a). Sequence analysis of slb^{tx226} and slb^{tz216} alleles revealed point mutations at positions Trp 234 and Gly 155, introducing in-frame stop codons that result in truncation of the Wnt11 protein (Fig. 1b). These mutations would be expected to generate non-functional proteins (see below), so both alleles are likely to be null mutations.

Expression analysis of *wnt11* in wild-type and $slb^{-/-}$ embryos confirmed that Wnt11 is a good candidate for mediating Slb/Wnt11 activity. In wild-type embryos, *wnt11* expression is first detectable in the germring at the shield stage and subsequently in the paraxial head mesoderm and in the neuroectoderm (Fig. 1c–e and ref. 12). By late gastrulation, the paraxial head mesodermal domain lies directly anterior to presumptive paraxial somitic mesoderm and the lateral neuroectodermal domain is posterior to the presumptive forebrain (Fig. 1i–k and data not shown). In *slb* embryos, *wnt11* expression is initiated but is strongly downregulated in all expression domains by late gastrulation (Fig. 1f–h).

To confirm that the $slb^{-/-}$ phenotype is due to mutations in the *wnt11* gene, we overexpressed *wnt11* RNA in mutant and wild-type embryos. In uninjected $slb^{-/-}$ embryos, the prechordal plate is more elongated and the notochord is shorter and wider than in wild-type embryos, correlating with a partial fusion of the eyes at later developmental stages[2] (Fig. 2a, b, g, h). The injection of 10 pg of *wnt11* RNA into wild-type embryos at the one-cell stage had either little or no obvious effect, or caused defective morphogenesis of the

Table 1 *wnt11* and *dsh-ΔN* rescue the *slb* eye phenotype at pharyngula stage

RNA injected	Genotype	Wild type (%)	*slb* (%)	Reduced (%)	Total (*n*)
–	wild type	100	0	0	73
wnt11	wild type	66	0	34	69
wnt11(slb^{tx226})	wild type	100	0	0	30
–	*slb*	9	91	0	83
wnt11	*slb*	46	9	45	94
dsh-ΔN	*slb*	49	48	3	42
dsh-DEP+	wild type	5	45	50	37

10 pg of *wnt11* and *wnt11* (slb^{tx226}) RNA and 200 pg of *dsh-ΔN* and *dsh-DEP+* RNA were injected into one-cell-stage embryos. Eyes classified as '*slb*' showed some degree of cyclopia, and eyes classified as 'reduced' were reduced in size.

Table 2 *wnt11* and *dsh-ΔN* rescue the *slb* convergent extension phenotype at the tailbud stage

RNA injected	Genotype	Wild type (%)	*slb* (%)	Abnormal (%)	Total (*n*)
–	wild type	100	0	0	46
wnt11	wild type	74	0	26	43
wnt11(slb^{tx226})	wild type	100	0	0	41
–	*slb*	4	96	0	90
wnt11	*slb*	36	7	57	41
dsh-ΔN	*slb*	32	20	48	46
dsh-DEP+	wild type	0	40	60	54

10 pg of *wnt11* and *wnt11* (slb^{tx226}) RNA and 200 pg of *dsh-ΔN* and *dsh-DEP+* RNA were injected into one-cell-stage embryos. Embryos classified as '*slb*' displayed an elongated, posteriorly displaced prechordal plate and shortened notochord, and embryos classified as 'abnormal' showed other variable defects in morphogenesis of prechordal plate and notochord.